Extreme Mechanics Letters 40 (2020) 100896

Contents lists available at ScienceDirect

Extreme Mechanics Letters

journal homepage: www.elsevier.com/locate/eml

Optimal design of phononic media through genetic algorithm-informed pre-stress for the control of antiplane wave propagation

Riccardo De Pascalis [a,*], Teresa Donateo [a], Antonio Ficarella [a], William J. Parnell [b]

[a] Department of Engineering for Innovation, University of Salento, 73100 Lecce, Italy
[b] Department of Mathematics, University of Manchester, Oxford Road, Manchester M13 9PL, UK

ARTICLE INFO

Article history:
Received 11 June 2020
Received in revised form 13 July 2020
Accepted 17 July 2020
Available online 23 July 2020

Keywords:
Band gap
Tunable
Antiplane waves
Pre-stress
Genetic algorithm
Phononic crystal

ABSTRACT

In this paper we employ genetic algorithms in order to theoretically design a range of phononic media that can act to prevent or ensure antiplane elastic wave propagation over a specific range of low frequencies, with each case corresponding to a specific pre-stress level. The medium described consists of an array of cylindrical annuli embedded inside an elastic matrix. The annuli are considered as capable of large strain and their constitutive response is described by the popular Mooney–Rivlin strain energy function. The simple nature of the medium described is an alternative approach to topology optimization in phononic media, which although useful, often gives rise to complex phase distributions inside a composite material, leading to more complicated manufacturing requirements.

Phononic crystals (PCs) represent an important class of materials that can be employed in various applications pertaining to the control of the propagation of sound and vibration [1,2]. In particular the choice of microstructural lengthscales, distribution of microstructure and periodicity of the medium in question, coupled with the choice of materials employed allows one to carefully control the pass bands and band gaps of the material, with the latter corresponding to ranges of frequency where waves cannot propagate in the medium. Since the pioneering work that showed that the same analysis for photonics applies to phononics [3,4] there has been a huge range of research investigating the properties of PCs [5].

Since the early 2000s a significant branch of the field has focussed on the optimal design of PCs, often via a multi-objective approach. One mechanism for this is to employ classical optimization techniques, which appear to have been first used to maximize band-gap widths in [6]. This work employed classical finite element computations for cell problems, combined with the method of moving asymptotes. Approaches that employed genetic algorithms first arose in 2006 and 2007 [7–9]. Genetic algorithms (GAs) are metaheuristic, nature-inspired optimization methods that mimic the natural evolution of species working on a population of candidate solutions that evolves through a predefined number of generations. They are robust (guarantee convergence), general (can be applied to any type of problems and without any restrictions on the form of objective and constraint functions), easy to use and implicitly parallel (they can handle multi-objective optimization problems). On the other hand, their accuracy increases with the size of the population and the number of generations. Therefore, they require a larger computational time with respect to classical methods, particularly when the number of design parameters and optimization goals is very high. Given their benefits however they are one of the most widely used optimization tools in engineering design problems [10].

Moving on then to the use of GAs in PC design, in [7] GA optimization was considered in the case of acoustics for two-dimensional PCs. Finite element methods were coupled with GAs for two phase materials. Layered materials were considered in [8] and antiplane waves in fibrous materials in [9]. In all of these works, the material properties of both phases are fixed prior to optimization. Layered photonic structures were optimized by the use of GAs in [11]. In [12,13] GAs were employed to maximize the width of elastic band-gaps for two-dimensional PCs associated with either in-plane waves or antiplane waves and also to control both wave types. In particular [13] employed voided materials, with the follow up study in [14] describing a multi-objective method that optimized band-gap width whilst minimizing mass. Alternative computational approaches are described in the more recent optimization studies of [15–18] with the latter considering

* Corresponding author.
E-mail addresses: riccardo.depascalis@unisalento.it (R. De Pascalis), teresa.donateo@unisalento.it (T. Donateo), antonio.ficarella@unisalento.it (A. Ficarella), William.J.Parnell@manchester.ac.uk (W.J. Parnell).

https://doi.org/10.1016/j.eml.2020.100896

thin-walled structures, of potential use in low-loss ultrasound devices. Optimizing three-phase PCs using GAs was the focus of the study in [19]. More broadly, genetic algorithms and general optimization techniques have become popular in the context of wave propagation and metamaterials in recent years see e.g. [20–22].

PC materials designed using the above techniques are optimal but have the disadvantage that once designed their properties are fixed. The notion of *reconfigurable* or *tunable* PCs and metamaterials has therefore evolved as a separate research field in recent years [23]. The first work in this field noted that the band gaps of PCs could be modified by elastic pre-stress [24–26] and since then a plethora of mechanisms have been shown to affect band-gap location and width [27–34]. It has also been shown that, perhaps surprisingly, some materials can be designed whose band gaps are invariant to deformation [35,36]. Furthermore, recently work has emerged that exploits pre-stress in order to design one-way wave propagation devices [37,38].

The motivation for the present work is to design *optimal* materials for the control of antiplane waves via the choice of pre-stress mechanisms. Very little research has been carried out to optimize band gaps in the presence of pre-stress, using GAs. An important exception is the work carried out in [39] which considers the optimization of antiplane wave band gaps via GAs in a dielectric elastomer at fixed imposed voltage via the unit cell topology (phase distribution). The aim in the present paper is to employ a relatively "simple" structure without the need to design and manufacture complex phase topology. We then use pre-stress to both open up wide low frequency band-gaps at specific pre-stress levels and at other pre-stress levels to close these gaps entirely so that a complete pass band material results. Such a material therefore has the potential to act as a filter. For reasons of stability, the fibrous material described is discussed in the context when the fibres are stretched axially ($\lambda > 1$, where λ is the principal axial stretch). The analysis could certainly be repeated considering $\lambda < 1$, but in this case the algorithm would have to take into account the fact that at critical loads/stretches the cylinder will buckle [40,41]. This would change completely the periodic structure although such snap-through bifurcations have been employed in order to switch wave propagation mechanisms entirely [42]. The method introduced here, associated with the stretch of periodically distributed cylindrical annuli embedded in a matrix material, is described in the context of antiplane shear waves but it can also be deployed to optimize more complex in-plane elastic wave propagation [32].

1. Antiplane waves in pre-stressed phononic media

We follow the notation in [35] and consider the propagation of linear elastic antiplane waves, polarized in the Z direction and propagating in the XY plane. It will be convenient to formulate the problem in circular cylindrical polar coordinates and therefore defining these via $X = R\cos\Theta, Y = R\sin\Theta$, and assuming that the wave (displacement w in the Z direction) takes the time-harmonic form $\Re[w(X,Y)e^{-i\omega t}]$, where ω is the circular frequency, w is then governed by the harmonic wave equation [35,43]

$$\frac{1}{R}\frac{\partial}{\partial R}\left(R\frac{\partial w}{\partial R}\right)+\frac{1}{R^2}\frac{\partial^2 w}{\partial \Theta^2}+\frac{\rho}{\mu}\omega^2 w=0 \tag{1}$$

in an unstressed configuration where ρ is the mass density and μ is the linear infinitesimal shear modulus of the medium.

We now consider antiplane waves propagating in the medium as depicted in the upper part of Fig. 1. This medium consists of a homogeneous material having mass density ρ_0 and shear modulus μ_0 having a square periodic array (of period ℓ) of cylindrical

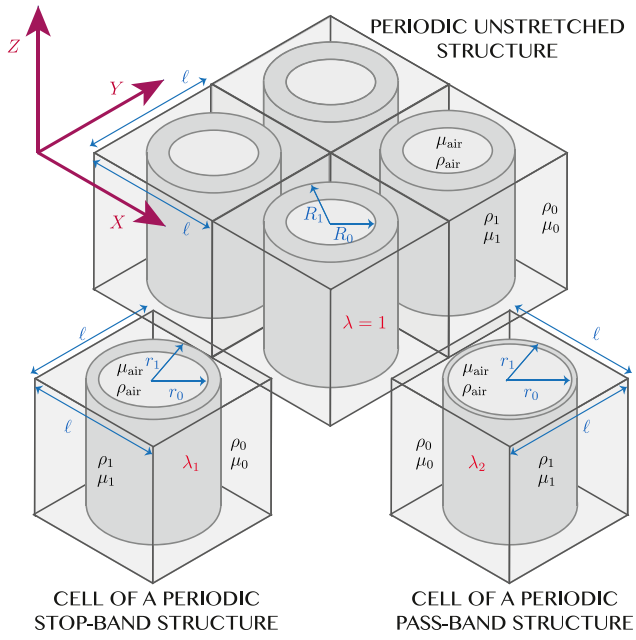

Fig. 1. Figure illustrating the geometry and the material properties of the periodic structure with no pre-stress (equivalently $\lambda = 1$, where λ is the axial pre-stretch in each cylindrical annulus) which for the same material and geometric properties can become a stop-band device ($\lambda = \lambda_1$) and pass band device ($\lambda = \lambda_2$) at appropriately chosen stretches.

voids, each of radius R_1 distributed inside the material. These voids are each filled with a cylindrical annulus of a nonlinearly elastic incompressible medium having initial outer radius R_1 and inner radius R_0. Given its nonlinear nature this annulus can be deformed both axially and radially, being subject to large deformation as shown in the following paragraphs, but we always require that its outer radius remains as $r_1 = R_1$ when waves propagate through the medium. Under this deformation the inner radius becomes r_0. The annulus has linear elastic shear modulus $\mu_1 < \mu_0$ and mass density $\rho_1 < \rho_0$. In the undeformed configuration each cylinder therefore resides in the domain $R_0 \le R \le R_1$, and Θ in $[0, 2\pi)$ (where these coordinates are prescribed locally in each cell). The initial deformation of the cylindrical annulus is prescribed by imposing an external pressure p_0 on the inner surface $R = R_0$ *or equivalently* by imposing an axial stretch λ along the Z direction. The deformation that ensures this pre-deformation in the case of incompressible materials is given by [44,45]

$$R(r)=\sqrt{\lambda(r^2+M)},\quad \Theta=\theta,\quad Z=\frac{1}{\lambda}z \tag{2}$$

where (r,θ,z) are cylindrical coordinates in the deformed configuration, and $M = \left(\frac{1}{\lambda}-1\right)R_1^2$. The form of the function $R(r)$ is determined by imposing the constraint of incompressibility $\lambda_r\lambda_\theta\lambda_z = 1$. We also have the additional constraints

$$R_0 = R(r_0),\quad R_1 = R(r_1) = r_1. \tag{3}$$

The principal stretches in the direction r,θ and z are $\lambda_r = 1/R'(r)$, $\lambda_\theta = r/R(r)$ and $\lambda_z = \lambda$ respectively. Moreover the single nontrivial balance equation allows the determination of the radial component of the Cauchy stress as

$$T_{rr} = -p_0 + \int_{r_0}^{r}\frac{1}{s}\left(\lambda_\theta(s)\frac{\partial \mathcal{W}}{\partial \lambda_\theta}-\lambda_r(s)\frac{\partial \mathcal{W}}{\partial \lambda_r}\right)ds, \tag{4}$$

where $\mathcal{W} = \mathcal{W}(\lambda_r,\lambda_\theta,\lambda_z)$ is the strain energy function that describes the constitutive behaviour of the nonlinearly elastic

annulus and $T_{rr}(r_0) = -p_0$ and $T_{rr}(r_1) = 0$ [46]. Expression (4) is deduced from the radial equilibrium equation by expressing all relations for stress in terms of the strain energy function except for the term dT_{rr}/dr. Integration between r_0 and some point $r \in [r_0, r_1]$ yields this expression.

At this point it is worth noting that these annuli deform whilst embedded inside an elastic matrix which *does not* undergo any pre-stress. That this is possible is due to the fact that the exterior radius of the cylinders in question remain fixed as described above. On a practical level we anticipate that the annuli and matrix are not bonded but are instead in close contact. When pre-stressing the annuli, pressure can be evacuated from the interior region, decreasing the exterior radius, an axial stretch imposed and then the core is re-pressurized to ensure contact with the matrix domain once again. This may mean a small region of pre-stress in the matrix close to the contact at R_1 but its stiffer nature ($\mu_1 < \mu_0$) will ensure that this region is limited.

The equation governing the propagation of small amplitude antiplane waves propagating through the medium just described consisting of an unstressed host medium and periodically spaced pre-stressed cylindrical annuli, as depicted in Fig. 1, can be shown to be [47,46,35]

$$\frac{1}{r}\frac{\partial}{\partial r}\left(r\mu_r(r)\frac{\partial w}{\partial r}\right) + \frac{\mu_\theta(r)}{r^2}\frac{\partial^2 w}{\partial \theta^2} + \rho\omega^2 w = 0, \tag{5}$$

where

$$\rho = \begin{cases} \rho_{\text{air}} & r < r_0 \\ \rho_1 & r_0 \le r \le r_1 \\ \rho_0 & r > r_1 \end{cases} \tag{6}$$

is the mass density of the medium (the annulus density is unaffected by the pre-deformation given that the material is incompressible) and where the incremental shear modulus in the annulus region is

$$\mu_r(r) = \left(\frac{\lambda_r \mathcal{W}_r - \lambda_z \mathcal{W}_z}{\lambda_r^2 - \lambda_z^2}\right)\lambda_r^2, \tag{7}$$

$$\mu_\theta(r) = \left(\frac{\lambda_\theta \mathcal{W}_\theta - \lambda_z \mathcal{W}_z}{\lambda_\theta^2 - \lambda_z^2}\right)\lambda_\theta^2 \tag{8}$$

where $\mathcal{W}_r, \mathcal{W}_\theta$ and $\mathcal{W}_z$ denote $\partial\mathcal{W}/\partial\lambda_r$, $\partial\mathcal{W}/\partial\lambda_\theta$ and $\partial\mathcal{W}/\partial\lambda_z$ respectively. For ease of reference, note in particular that the form of the incremental equation and moduli for the antiplane problem is given in Appendix A of [47]. In the case of no deformation $\lambda = 1$, the incremental moduli each reduce to the constant $\mu_r = \mu_\theta = \mu_1$. In the interior of the annulus ($r < r_0$) $\mu_r = \mu_\theta = \mu_{\text{air}}$ and in the host ($r > r_1$ with r inside the periodic square cell) $\mu_r = \mu_\theta = \mu_0$.

One of the most popular strain energy functions used to describe incompressible hyperelastic materials is the Mooney–Rivlin model [48]

$$\mathcal{W}_{\text{MR}} = \frac{\mu}{2}\Big[S_1\left(\lambda_r^2 + \lambda_\theta^2 + \lambda_z^2 - 3\right) + (1 - S_1)\left(\lambda_r^2\lambda_\theta^2 + \lambda_r^2\lambda_z^2 + \lambda_\theta^2\lambda_z^2 - 3\right)\Big] \tag{9}$$

where $0 < S_1 \le 1$ is a constant. Typically in "real" materials $S_1 \in [0.6, 1]$ (e.g [49,50]) and when $S_1 = 1$ the model reduces to the classical neo-Hookean model [51]

$$\mathcal{W}_{\text{NH}} = \frac{\mu}{2}\left(\lambda_r^2 + \lambda_\theta^2 + \lambda_z^2 - 3\right). \tag{10}$$

For the Mooney–Rivlin model, the incremental moduli reduce to the forms

$$\mu_r^{\text{MR}}(r) = \mu_1\frac{R^2 S_1 - r^2(S_1 - 1)}{\lambda^2 r^2}, \tag{11}$$

$$\mu_\theta^{\text{MR}}(r) = \mu_1\left(\frac{r^2 S_1}{R^2} + \frac{1 - S_1}{\lambda^2}\right), \tag{12}$$

where $R = R(r)$ is given in (2).

2. Plane wave expansion

We seek solutions to (5) in the periodic medium via the Plane Wave Expansion (PWE) method, which as reported in [35] allows the straightforward determination of the band-gap spectrum via the numerical solution of the eigenvalue problem. This eigenvalue problem results from the PWE scheme via a representation of the displacement as a sum of plane waves modulated by a Bloch phase term in order to ensure quasi-periodicity of the propagating wave. The complex displacement w is written in the form

$$w(\mathbf{x}) = e^{i\mathbf{K}\cdot\mathbf{x}}\sum_{\mathbf{G}} W(\mathbf{G})e^{i\mathbf{G}\cdot\mathbf{x}} \tag{13}$$

where $\mathbf{K}$ is the Bloch wavevector, $\mathbf{G}$ are the reciprocal lattice vectors $\mathbf{G} = 2\pi/\ell(m\mathbf{e}_x + n\mathbf{e}_y)$, with m, n integers and $\mathbf{e}_x, \mathbf{e}_y$ unit vectors and $W(\mathbf{G})$ are the Fourier coefficients of the displacement. It is most convenient to express Eq. (5) in Cartesian coordinates for the purposes of the computations [35].

The frequencies ω can be obtained from the generalized eigenvalue problem which will give the full dispersion relation associated with the medium, referring the reader to [2] for general details and to [35] where a description of the specific problem above is provided. The frequency of the jth mode is denoted by ω_j which is ordered with respect to increasing j, i.e. $\omega_j < \omega_{j+1}, j = 1, 2, \ldots$. We scan the wavenumber around the edge of the irreducible Brillouin zone (see Fig. 2) with the three boundaries denoted by $\mathbf{K} = (0\mathbf{i} + 0\mathbf{j})/\ell \to \Gamma$, $\mathbf{K} = (0.5\mathbf{i} + 0\mathbf{j})/\ell \to X$ and $\mathbf{K} = (0.5\mathbf{i} + 0.5\mathbf{j})/\ell \to M$. For further details as to how this method is employed for pre-stressed configurations we refer the reader to [35] and for more general details about the method to [2].

Our interest here is to employ GAs in order to find optimal structures in specific pre-stressed states and in particular which pre-stretch, say $\lambda = \lambda_1$, provides the widest band gap in a given frequency range say $\omega \in \Omega_1 \subset \Omega$, where Ω contains the first three modes. Additionally, this same structure should have no band gaps in Ω_1 at an alternative stretch $\lambda = \lambda_2$.

3. Optimization function for the genetic algorithm

Scanning for $\mathbf{K} \in [M - \Gamma - X - M]$ and considering the analysis for the first three dispersion curves, the goal of the single-objective optimization is to find optimal values for the parameter set $\mathcal{P} = \{R_0, \mu_1, \rho_1, S_1\}$ from the set of possible choices, i.e.

$$\mathcal{A} = \{R_0 \in (0, R_1), \mu_1 \in \mu_0[10^{-3}, 1], \rho_1 \in \rho_0[10^{-3}, 1], S_1 \in [0.6, 1]\} \tag{14}$$

noting that we have chosen annuli that are softer than the matrix, consistent with the assumption that the annuli are nonlinear and capable of large deformation, whereas the matrix is a stiffer medium hosting these annuli. These parameters are then chosen to optimize the phononic material under study by satisfying the following objective

$$\text{O}: \max_{\mathcal{A}, \lambda_1, j=1,2} \Phi, \tag{15}$$

where

$$\Phi = 2\frac{\min_{\mathbf{K}}\omega_{j+1}^2(\mathbf{K}) - \max_{\mathbf{K}}\omega_j^2(\mathbf{K})}{\min_{\mathbf{K}}\omega_{j+1}^2(\mathbf{K}) + \max_{\mathbf{K}}\omega_j^2(\mathbf{K})} \tag{16}$$

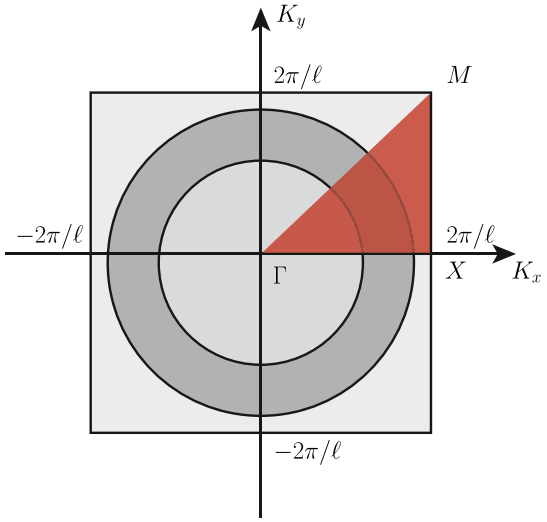

Fig. 2. The irreducible Brillouin zone of the cell is emphasized in red. (For interpretation of the references to colour in this figure legend, the reader is referred to the web version of this article.)

is the objective function given and employed in the pioneering work [6]. In (16) $\min_{\mathbf{K}} \omega_j^2(\mathbf{K})$ and $\max_{\mathbf{K}} \omega_j^2(\mathbf{K})$ denote the minimum and the maximum, respectively, of the square of the jth frequency ω_j^2 over the entire discrete $\mathbf{K}$ spanning the border of the triangle ΓXM representing the irreducible Brillouin zone (see Fig. 2). This optimization is therefore set up to try to maximize the relative band-gap size between the jth and $(j+1)$th dispersion curves by maximizing the lowest frequency of the overlying bands and minimizing the highest frequency of the underlying bands. The particular band gap width is normalized with respect to its mid frequency.

Note that a band gap exists only when the minimum of the $(j+1)$th eigenfrequency is greater than the maximum of the jth eigenfrequency. If this does not occur for a specific configuration, Φ is set to zero. Furthermore, we subject the solutions of the optimization in (15) to two further constraints:

$$\mathcal{C}_1 : \max_{\mathcal{P},\lambda_2,j=1,2} \Phi = 0, \tag{17}$$

$$\mathcal{C}_2 : \max_{\mathcal{P},\lambda_2} \omega_3 \geq \min_{\mathcal{P},\lambda_1} \omega_{\bar{j}+1} \tag{18}$$

with $\bar{j} = j$ as chosen in the optimization (15). The two conditions $\mathcal{C}_{1,2}$ ensure that for the stretch $\lambda = \lambda_2$, waves will always propagate in the frequency range $\omega \in \Omega_1$, noting that Ω_1 is the range of frequencies which contains the widest possible band gap at stretch $\lambda = \lambda_1$.

The flow chart of the optimization process is shown in Fig. 3. The GA used in this work is the NSGA-II (non dominated sorting genetic algorithm) implemented in the Esteco-Modefrontier optimization software. The algorithm starts with an initial population of 200 individuals obtained with a Sobol design of experiments after selecting, for each variable, the range and the step of variation shown in Table 1. The maximum number of generations was set equal to 200 while the crossover and mutation probability were 0.5 and 0.02, respectively. The elitism operator allowed the best individual of each generation to be copied in the next generation without modifications [52,53].

4. Results

Results are presented in nondimensional form by introducing the following scaled variables, non-dimensionalized on the properties of the matrix material

$$\hat{\mu}_1 = \frac{\mu_1}{\mu_0}, \quad \hat{\mu}_{\text{air}} = \frac{\mu_{\text{air}}}{\mu_0}, \tag{19}$$

$$\hat{\rho}_1 = \frac{\rho_1}{\rho_0}, \quad \hat{\rho}_{\text{air}} = \frac{\rho_{\text{air}}}{\rho_0} \tag{20}$$

and furthermore

$$\hat{\mathbf{K}} = \ell\mathbf{K}, \quad \hat{R} = \frac{R}{\ell}, \quad \hat{r} = \frac{r}{\ell}, \quad \hat{\omega} = \frac{\ell\omega}{c_0} \tag{21}$$

where $c_0 = \sqrt{\mu_0/\rho_0}$ is the shear wave speed in the host material and where we fix $\hat{R}_1 = R_1/\ell = 0.45$. Since the associated material parameters for the air region inside the deformable cylindrical annuli are negligible with respect to the matrix parameters, we set them to be $\hat{\mu}_{\text{air}} = \hat{\rho}_{\text{air}} = 10^{-8}$. We also checked that the routine is stable for choices smaller than this. As noted above we anticipate that the annulus material will be softer than the matrix and hence the choice of relative shear moduli.

Details of the PWE numerical scheme procedure which is now implemented within the context of the GA are provided in [35]. Parameters in $\mathcal{P}$ and the stretches λ_1, λ_2 are varied in the ranges and with increments according to Table 1. Moreover, here, given that the parameter ranges are wider than that studied in [35], in order to ensure numerical stability and robust optimization, we increased the maximum plane wave number to $N = 15$ (corresponding to 961 plane waves). This is an increase from the choice $N = 10$ (corresponding to 441 plane waves) which was quoted in [35] as a limit that ensured sufficiently accurate results.

We run the GA separately for the Neo-Hookean (NH) model ($S_1 = 1$) and for the Mooney–Rivlin material (MR) case with $S_1 \in [0.6, 1]$ so that in the latter the parameter S_1 serves as an additional optimization mechanism. The algorithm chooses λ_1 to maximize Φ and (for the same material constants) λ_2 to satisfy the constraints $\mathcal{C}_1, \mathcal{C}_2$ in (17)–(18).

As explained above, 200 generations for each model were performed by the NSGA-II algorithm with a population of 200 individuals. Therefore, the total number of designs to be analysed by the method was nominally 40,000. We summarize the convergence towards the maximum value of the optimization function for both the NH and MR models in Table 2.

We can therefore conclude that the algorithm was efficient in this application and in fact it required a very low number of evaluations with respect to the total number of possible combinations of the input parameters and reached convergence long before the pre-fixed number of generations.

Table 1
Parameters ranges and respective step of variation.

VAR	MIN	MAX	STEP
$\hat{R}_0$	0.01	0.44	0.01
$\log \hat{\mu}_1$	−3	0	0.01
$\log \hat{\rho}_1$	−3	0	0.01
λ_1	1	7	0.1
λ_2	1	7	0.1
S_1(MR)	0.6	1	0.01
S_1(NH)	1	1	–

Table 2
Convergence values where 'NG' stays for the generation at which optimum has been detected, 'NC' number of analysed candidates (net of repeated designs) and 'NCF' the number of feasible designs among 'NC'.

MODEL	NG	NC	NCF
NH	144	5247	1923
MR	90	5138	3469

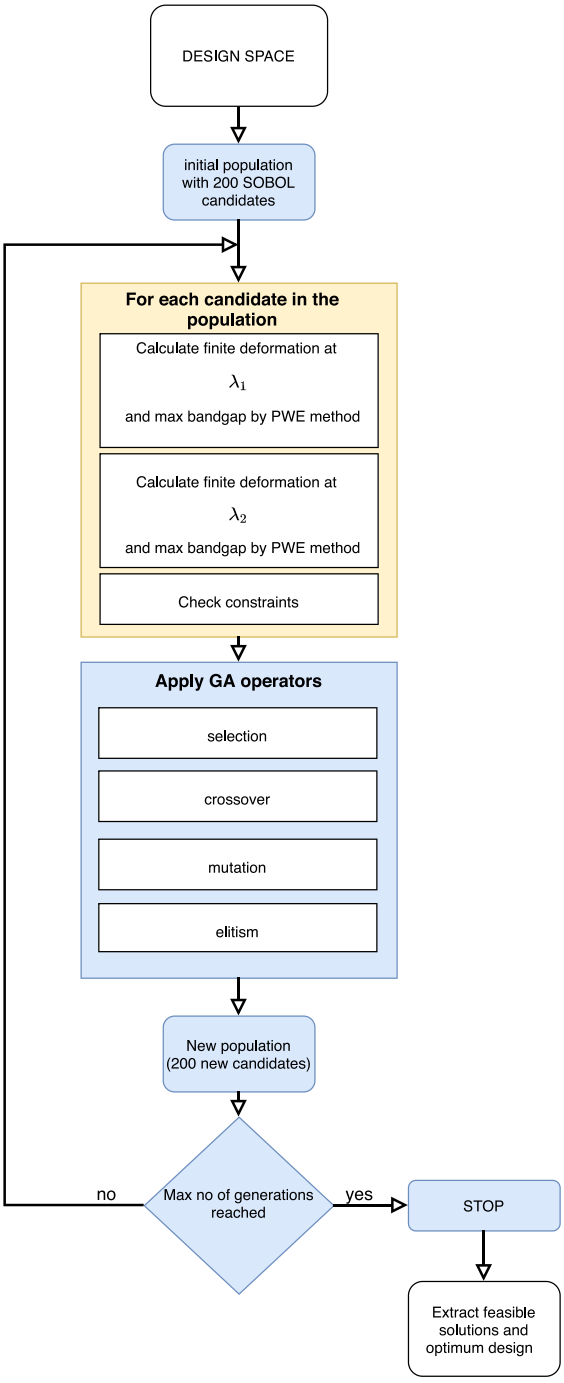

Fig. 3. Flow chart of the Genetic Algorithm optimization process.

The process above provides a rich set of data from which to design potentially interesting phononic media. Such potential solutions are defined as *feasible* in the sense that for the material parameters in question both constraints $\mathcal{C}_1$ and $\mathcal{C}_2$ are satisfied. This ensures that such a material with parameters $\mathcal{P}$ can act as a tunable wave filter by imposing only pre-stress in the annulus regions. These feasible solutions, illustrated as filled, coloured circles in Figs. 4, 5 are distinguished from the open circle *unfeasible* solutions covering the rest of the parameter space of interest, which initiate the algorithm. The colours of the filled circles, as illustrated in the colour bar, express the corresponding $\Phi \in [0, 1]$ associated with the choice of λ_1.

The results obtained illustrate that for both neo-Hookean (Fig. 4) and Mooney–Rivlin (Fig. 5) models we are able to achieve the main goal of obtaining phononic materials with fixed material parameters that behave simultaneously as having wide stop-bands ($\lambda = \lambda_1$) and entire pass-bands ($\lambda = \lambda_2$) for a given frequency range by imposing pre-stress alone in the annulus regions. Figs. 4 and 5(a) and (b) are associated with material properties and initial annulus inner radius that enable feasible choices, with each of these cases corresponding to pairs of stretches that are plotted in (c). In particular, we identify and plot an *optimal* result within the parameter space $\mathcal{P}$ and also another solution that is identified as, perhaps, more practical in the sense that the opening up of a wide low-frequency band gap is achieved at a lower stretch λ_1. The optimal solution, a black diamond corresponding to $\Phi \approx 0.78$ is plotted in each of the subfigures of Fig. 4. In Fig. 4(a), solutions that approach this

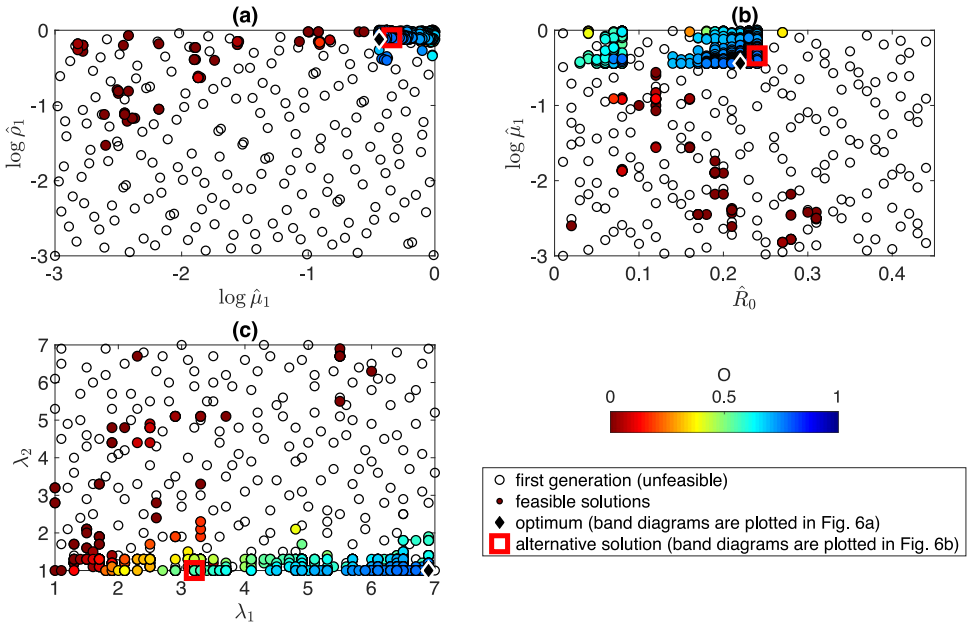

Fig. 4. Illustrating both unfeasible (unfilled circles) and feasible (filled, coloured circles) solutions found by the genetic algorithm for the neo-Hookean case. The colour of the filled circles for the feasible solutions is dictated by the colour bar, illustrating the range of associated $\Phi \in [0, 1]$, maximized by the choice of λ_1 for those material properties. The optimal solution (black diamond) is determined for the material configuration $\hat{R}_0 = 0.22, \hat{\mu}_1 = 10^{-0.44}, \hat{\rho}_1 = 10^{-0.12}$ coupled with imposed stretches $\lambda_1 = 6.9$ and $\lambda_2 = 1$. The "nearby" solution in a red squared box (in material configuration space) is $\hat{R}_0 = 0.24, \hat{\mu}_1 = 10^{-0.34}, \hat{\rho}_1 = 10^{-0.1}$ coupled with the (smaller) stretches $\lambda_1 = 3.2, \lambda_2 = 1$. (For interpretation of the references to colour in this figure legend, the reader is referred to the web version of this article.)

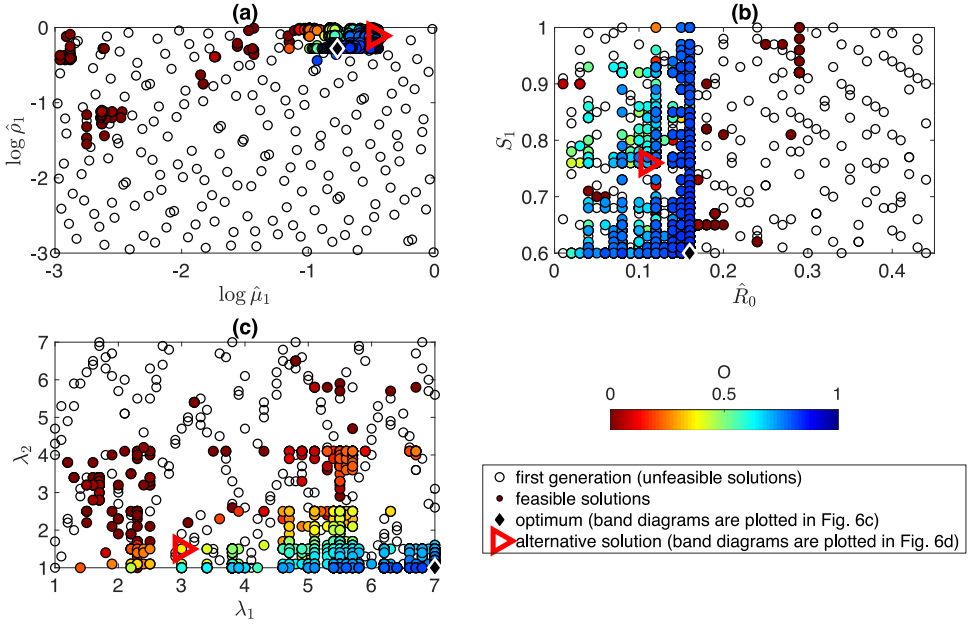

Fig. 5. Illustrating both unfeasible (unfilled circles) and feasible (filled, coloured circles) solutions found by the genetic algorithm for the Mooney–Rivlin case. The colour of the filled circles for the feasible solutions is dictated by the colour bar, illustrating the range of associated $\Phi \in [0, 1]$, maximized by the choice of λ_1 for those material properties. The optimal solution (black diamond) is determined for the material configuration $\hat{R}_0 = 0.16, \hat{\mu}_1 = 10^{-0.77}, \hat{\rho}_1 = 10^{-0.28}, S_1 = 0.6$ coupled with imposed stretches $\lambda_1 = 7$ and $\lambda_2 = 1$. An alternative solution is identified in a red triangular box as $\hat{R}_0 = 0.11, \hat{\mu} = 10^{-0.47}, \hat{\rho}_1 = 10^{-0.11}, S_1 = 0.76$ coupled with the (smaller) stretches $\lambda_1 = 3, \lambda_2 = 1.5$. (For interpretation of the references to colour in this figure legend, the reader is referred to the web version of this article.)

optimal result are typically located in the area $1/10 \leq \hat{\rho}_1, \hat{\mu}_1 \leq 1$. Fig. 4(b) illustrates that optimal results are found for smaller values of $\hat{R}_0$, thus avoiding thin annuli where instabilities could be a serious issue. Finally, Fig. 4(c) illustrates optimal results at specific stretches. This plot clearly illustrates that configurations with material properties such that λ_2 is close to unity (small stretch) are favoured in order to ensure a pass-band material, coupled with a larger stretch (λ_1) to achieve a stop-band at low frequency. This therefore suggests that it is in principle possible to manufacture a structure such that in its undeformed state it can ensure wave propagation in the frequency range $\hat{\Omega}_1$, whilst in its deformed state it would act to prevent wave propagation in that same frequency range. For neo-Hookean materials the optimal material properties are $\hat{R}_0 = 0.22$, $\hat{\mu}_1 = 10^{-0.44}$, $\hat{\rho}_1 =$

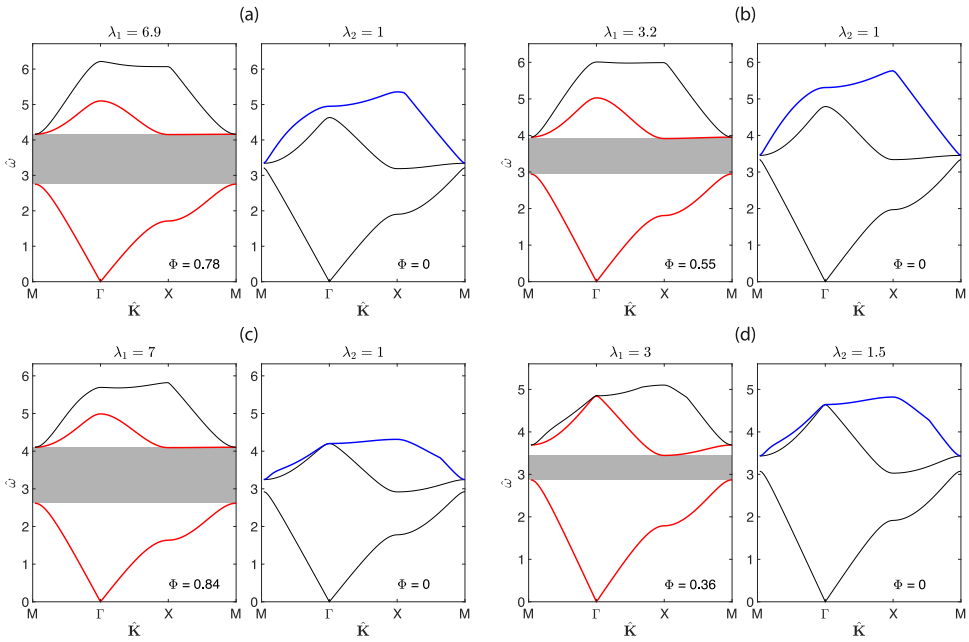

Fig. 6. Dispersion curves illustrating the opening up (choice of λ_1) and closing (choice of λ_2) of the lowest band gap. The top figures illustrate the neo-Hookean case for the optimal solution (a) $R_0 = 0.22$, $\mu_1 = 10^{-0.44}$, $\rho_1 = 10^{-0.12}$ and alternative solution (b) with $R_0 = 0.24$, $\mu_1 = 10^{-0.34}$, $\rho_1 = 10^{-0.1}$. The bottom figures illustrate the Mooney–Rivlin case for the optimal solution (c) $\hat{R}_0 = 0.16, \hat{\mu}_1 = 10^{-0.77}, \hat{\rho}_1 = 10^{-0.28}, S_1 = 0.6$ and alternative solution (d) $\hat{R}_0 = 0.11, \hat{\mu} = 10^{-0.47}, \hat{\rho}_1 = 10^{-0.11}, S_1 = 0.76$.

$10^{-0.12}$ coupled with imposed stretches $\lambda_1 = 6.9$ and $\lambda_2 = 1$. The associated dispersion curves for this case are plotted in Fig. 6(a). In (b) of the same figure we also plot the band structure for the alternative material choice $\hat{R}_0 = 0.24$, $\hat{\mu}_1 = 10^{-0.34}$, $\hat{\rho}_1 = 10^{-0.1}$ at (more practical) lower stretches $\lambda_1 = 3.2$ and $\lambda_2 = 1$.

Mooney–Rivlin optimal solutions plotted in Fig. 5 follow a similar trend to the Neo-Hookean results although, as expected, a little more spread of choices is here emphasized and the optimum (emphasized in the plots with a black diamond) for the MR is, at $\lambda = \lambda_1$, $\Phi \approx 0.84$ improving on that achieved for the NH case ($\Phi \approx 0.78$). The associated dispersion curves for the MR case are plotted in Fig. 6 (c, d) for the material choices $\hat{R}_0 = 0.16, \hat{\mu}_1 = 10^{-0.77}, \hat{\rho}_1 = 10^{-0.28}, S_1 = 0.6$ associated with the stretches $\lambda_1 = 7$ and $\lambda_2 = 1$ (c) and $\hat{R}_0 = 0.11, \mu = 10^{-0.47}, \rho_1 = 10^{-0.11}, S_1 = 0.76$ associated with the stretches $\lambda_1 = 3$ and $\lambda_2 = 1.5$ (d). In the MR case it is interesting to note that the latter case has some pre-stretch associated with the complete pass band medium.

The results illustrate that the 'best' feasible solutions all reside in the same regions of the parameter space considered, including the optimal stretches employed. Optimality appears to stem chiefly from the material configuration and geometry. This therefore promotes, facilitates and simplifies more practical aspects of phononic media design.

Generally the convergence of genetic algorithms towards optimal solutions can be difficult to achieve, particularly when the objective function (Φ in this case) is '*flat*' in the vicinity of the optimum and also when the problem involves a high number of design parameters in a limited region of feasibility. This problem is called GA-hardness [54]. In order to illustrate here that the method converged to such optimal solutions, we carried out a *local sensitivity analysis* in the region around the optimal solution, corresponding to the black diamond in Figs. 4–5 for the neo-Hookean and Mooney–Rivlin cases, respectively. To this end, small perturbations dx of each parameter and imposed stretch (corresponding to the step of variation as in the Table 1) around the optimum solution have been considered until it was verified that the objective function Φ is no longer increasing or unfeasible solutions are obtained. The results are shown in Fig. 7. We notice that the objective function is relatively flat with respect to $\hat{\mu}_1$ and $\hat{\rho}_1$ and this means that it is rather difficult for the algorithm to find the *global optimum*. This is more evident in the neo-Hookean model where, decreasing $\hat{\mu}_1$ by up to $5dx$, the objective function continues to increase with feasible solutions. The same effect is notable, but only up to $-dx$, for the parameter $\hat{\rho}_1$ in the neo-Hookean case. For all other design parameters, the local sensitivity analysis shows that it is not possible to obtain a further improvement in the fitness function by acting on that variable separately. Thus the convergence of the genetic algorithm can be said to be well-illustrated with respect to all parameters except $\hat{\mu}_1$ and $\hat{\rho}_1$. It should be noted however that the further improvements obtained with the sensitivity analysis with respect to these two variables can be said to be negligible from an engineering perspective. Indeed, considering for example the neo-Hookean case, $\hat{\mu}_1$ selected in Fig. 4 is $\hat{\mu}_1 = 10^{-0.44}$ while according to the plot in Fig. 7 an increment of $-5dx$ would take it to $\hat{\mu_1} = 10^{-0.49}$ with a discrepancy $\Delta \log \hat{\mu_1} \approx 0.04$ and a discrepancy in Φ of $|\Delta\Phi| \approx 0.06$.

5. Concluding remarks

The PC optimization process described above, through the use of genetic algorithms, illustrates how material parameters can be selected in order to guide the design of smart materials. These media are capable of behaving as stop-band or pass-band materials, employing the same physical and geometrical properties, simply by imposing different deformations in the cylindrical annuli, with the GAs permitting optimality.

The optimization has been carried out by allowing the model parameters (elastic and geometrical constants, applied stretches) vary over a finite but large window of possible values. This permits the materials engineer to optimize over a broad parameter space in order to design ideal, optimized materials, or perhaps close-to-ideal materials in more practical configurations.

Looking ahead to fabrication, recent advances in 3D printing [55–57] and the assumed periodicity of these smart materials

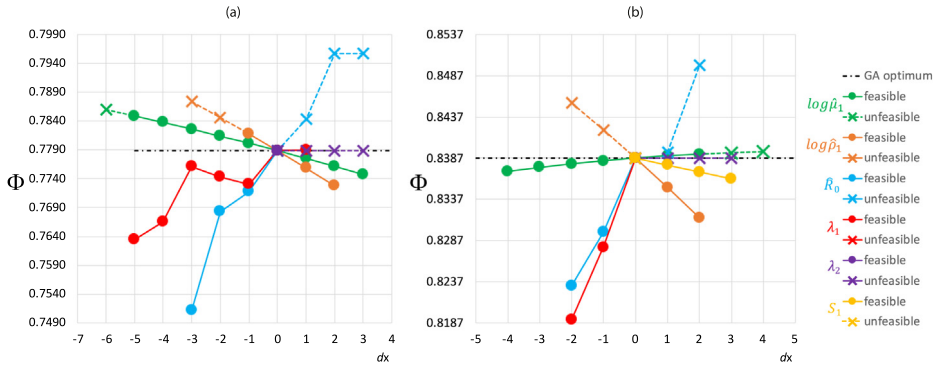

Fig. 7. Plot of Φ relative to the stretch λ_1 and to the optimum set of parameters (corresponding to the black diamond in Figs. 4–5 for the neo-Hookean (a) and Mooney–Rivlin case (b), respectively), varying each parameter by an increment dx corresponding to the step of variation as in Table 1 whilst others are kept fixed. (For interpretation of the references to colour in this figure legend, the reader is referred to the web version of this article.)

facilitate the manufacturing process. On the point of highly-deformable materials, it should be noted that we employed stretches up to $\lambda = 7$ in the present study motivated by the classical data of Treloar [51] on uniaxial extension of rubber and also to obtain a general indication of the trends of optimal solutions upon modifying imposed stretch. It is acknowledged that in practice, stretches are limited by the materials available and also on their constitutive models. We note however that there have been recent innovations in the development of highly stretchable materials [58] and this could become the key for permitting high annuli stretch. We highlight in Fig. 6(b) and (d) that one can still find "good" choices in terms of band gap optimization at smaller stretches. We further note the important property that results are relatively independent of the constitutive parameter S_1 in the Mooney–Rivlin model. This gives an indication of promise when employing more complex strain energy functions such as those described in [59].

The analysis described here can also be considered as opening up the possibility of designing a wide range of specific materials for various engineering applications, particularly in the broader context of more general elastic wave propagation or in the case where there is an interest in increasing the number of objectives over which the optimization takes place. This can be achieved via multi-objective optimization. Some examples of interest are, the potential to engineer the optimization of engine noise reduction with lighter materials [7,60]. Similarly in the acoustics context, porous and layered composites are used to efficiently absorb sound or for controlling the transmission and reflection of sound [61,62]. Controlling the volume fractions of inclusions and their properties in these materials also means tuning their microstructure and therefore their global response to propagating elastic waves. Finally, this design principle and the notion of materials reconfiguration is of significant interest in the context of more complex, non-periodic composites such as syntactic foams [63,64], the acoustic properties of which depend on their loading state. Properties can therefore be optimized by GA optimization to ensure a specific, highly tailored macromechanical response. These broader applications reveal the breadth of potential for the class of materials described here.

Declaration of competing interest

The authors declare that they have no known competing financial interests or personal relationships that could have appeared to influence the work reported in this paper.

Acknowledgement

Parnell is grateful to the Engineering and Physical Sciences Research Council (UK) for funding via grant EP/S019804/1.

References

[1] P.A. Deymier, Acoustic Metamaterials and Phononic Crystals, vol. 173, Springer Science & Business Media, 2013.
[2] V. Laude, Phononic Crystals: Artificial Crystals for Sonic, Acoustic, and Elastic Waves, vol. 26, Walter de Gruyter GmbH & Co KG, 2015.
[3] E. Yablonovitch, Photonic band-gap structures, J. Opt. Soc. Amer. B 10 (2) (1993) 283–295.
[4] M.S. Kushwaha, Classical band structure of periodic elastic composites, Internat. J. Modern Phys. B 10 (09) (1996) 977–1094.
[5] M.I. Hussein, M.J. Leamy, M. Ruzzene, Dynamics of phononic materials and structures: Historical origins, recent progress, and future outlook, Appl. Mech. Rev. 66 (4) (2014).
[6] O. Sigmund, J. Søndergaard Jensen, Systematic design of phononic band–gap materials and structures by topology optimization, Phil. Trans. R. Soc. A 361 (1806) (2003) 1001–1019.
[7] G.A. Gazonas, D.S. Weile, R. Wildman, A. Mohan, Genetic algorithm optimization of phononic bandgap structures, Int. J. Solids Struct. 43 (18) (2006) 5851–5866.
[8] M.I. Hussein, K. Hamza, G.M. Hulbert, R.A. Scott, K. Saitou, Multiobjective evolutionary optimization of periodic layered materials for desired wave dispersion characteristics, Struct. Multidiscip. Optim. 31 (1) (2006) 60–75.
[9] M.I. Hussein, K. Hamza, G.M. Hulbert, K. Saitou, Optimal synthesis of 2D phononic crystals for broadband frequency isolation, Waves Random Complex Media 17 (4) (2007) 491–510.
[10] X.-S. Yang, Genetic algorithms, in: X.-S. Yang (Ed.), Nature-Inspired Optimization Algorithms, Elsevier, Oxford, 2014, pp. 77–87, Chapter 5.
[11] J. Xu, Optimization of construction of multiple one-dimensional photonic crystals to extend bandgap by genetic algorithm, J. Lightwave Technol. 28 (7) (2010) 1114–1120.
[12] O.R. Bilal, M.I. Hussein, Optimization of phononic crystals for the simultaneous attenuation of out-of-plane and in-plane waves, in: Mechanics of Solids, Structures and Fluids; Vibration, Acoustics and Wave Propagation, in: ASME International Mechanical Engineering Congress and Exposition, vol. 8, 2011, pp. 969–972.
[13] O.R. Bilal, M.I. Hussein, Ultrawide phononic band gap for combined in-plane and out-of-plane waves, Phys. Rev. E 84 (6) (2011) 065701.
[14] H.-W. Dong, Y.-S. Wang, Y.-F. Wang, C. Zhang, Reducing symmetry in topology optimization of two-dimensional porous phononic crystals, AIP Adv. 5 (11) (2015) 117149.
[15] H.-W. Dong, X.-X. Su, Y.-S. Wang, Topology optimization of two-dimensional phononic crystals using FEM and genetic algorithm, in: 2012 Symposium on Piezoelectricity, Acoustic Waves, and Device Applications, SPAWDA, 2012, pp. 45–48.
[16] Y. Huang, S. Liu, J. Zhao, Optimal design of two-dimensional band-gap materials for uni-directional wave propagation, Struct. Multidiscip. Optim. 48 (3) (2013) 487–499.
[17] Z.-f. Liu, B. Wu, C.-f. He, Band-gap optimization of two-dimensional phononic crystals based on genetic algorithm and FPWE, Waves Random Complex Media 24 (3) (2014) 286–305.
[18] S. Hedayatrasa, K. Abhary, M.S. Uddin, J.K. Guest, Optimal design of tunable phononic bandgap plates under equibiaxial stretch, Smart Mater. Struct. 25 (5) (2016) 055025.
[19] W. Xu, J. Ning, M. Zhang, W. Wang, T. Yang, Three-phase microstructure topology optimization of two-dimensional phononic bandgap materials using genetic algorithms, Acta Mech. Solida Sin. 31 (6) (2018) 775–784.
[20] H.-W. Dong, S.-D. Zhao, P. Wei, L. Cheng, Y.-S. Wang, C. Zhang, Systematic design and realization of double-negative acoustic metamaterials by topology optimization, Acta Mater. 172 (2019) 102–120.

[21] X.K. Han, Z. Zhang, Topological optimization of phononic crystal thin plate by a genetic algorithm, Sci. Rep. 9 (1) (2019) 1–13.
[22] L. Pomot, C. Payan, M. Remillieux, S. Guenneau, Acoustic cloaking: Geometric transform, homogenization and a genetic algorithm, Wave Motion 92 (2020) 102413.
[23] Y.-F. Wang, Y.-Z. Wang, B. Wu, W. Chen, Y.-S. Wang, Tunable and active phononic crystals and metamaterials, Appl. Mech. Rev. 72 (4) (2020).
[24] W.J. Parnell, Effective wave propagation in a prestressed nonlinear elastic composite bar, IMA J. Appl. Math. 72 (2) (2007) 223–244.
[25] D. Bigoni, M. Gei, A.B. Movchan, Dynamics of a prestressed stiff layer on an elastic half space: filtering and band gap characteristics of periodic structural models derived from long-wave asymptotics, J. Mech. Phys. Solids 56 (7) (2008) 2494–2520.
[26] K. Bertoldi, M.C. Boyce, Mechanically triggered transformations of phononic band gaps in periodic elastomeric structures, Phys. Rev. B 77 (5) (2008) 052105.
[27] Y. Wang, F. Li, Y. Wang, K. Kishimoto, W. Huang, Tuning of band gaps for a two-dimensional piezoelectric phononic crystal with a rectangular lattice, Acta Mech. Sinica 25 (1) (2009) 65–71.
[28] G. Shmuel, G. deBotton, Band-gaps in electrostatically controlled dielectric laminates subjected to incremental shear motions, J. Mech. Phys. Solids 60 (11) (2012) 1970–1981.
[29] L. Wang, K. Bertoldi, Mechanically tunable phononic band gaps in three-dimensional periodic elastomeric structures, Int. J. Solids Struct. 49 (19–20) (2012) 2881–2885.
[30] Z. Xu, F. Wu, Z. Guo, Shear-wave band gaps tuned in two-dimensional phononic crystals with magnetorheological material, Solid State Commun. 154 (2013) 43–45.
[31] P. Zhang, W.J. Parnell, Band gap formation and tunability in stretchable serpentine interconnects, J. Appl. Mech. 84 (9) (2017).
[32] E.G. Barnwell, W.J. Parnell, I.D. Abrahams, Tunable elastodynamic band gaps, Extreme Mech. Lett. 12 (2017) 23–29.
[33] R. Getz, G. Shmuel, Band gap tunability in deformable dielectric composite plates, Int. J. Solids Struct. 128 (2017) 11–22.
[34] W.J. Parnell, R. De Pascalis, Soft metamaterials with dynamic viscoelastic functionality tuned by pre-deformation, Phil. Trans. R. Soc. A 377 (2144) (2019) 20180072.
[35] E.G. Barnwell, W.J. Parnell, I.D. Abrahams, Antiplane elastic wave propagation in pre-stressed periodic structures; tuning, band gap switching and invariance, Wave Motion 63 (2016) 98–110.
[36] P. Zhang, W.J. Parnell, Soft phononic crystals with deformation-independent band gaps, Proc. R. Soc. Lond. Ser. A Math. Phys. Eng. Sci. 473 (2200) (2017) 20160865.
[37] B.M. Goldsberry, S.P. Wallen, M.R. Haberman, Non-reciprocal wave propagation in mechanically-modulated continuous elastic metamaterials, J. Acoust. Soc. Am. 146 (1) (2019) 782–788.
[38] Y. Wang, W. Zhao, J.J. Rimoli, R. Zhu, G. Hu, Prestress-controlled asymmetric wave propagation and reciprocity-breaking in tensegrity metastructure, Extreme Mech. Lett. (2020) 100724.
[39] E. Bortot, O. Amir, G. Shmuel, Topology optimization of dielectric elastomers for wide tunable band gaps, Int. J. Solids Struct. 143 (2018) 262–273.
[40] A. Goriely, R. Vandiver, M. Destrade, Nonlinear Euler buckling, Proc. R. Soc. Lond. Ser. A Math. Phys. Eng. Sci. 464 (2099) (2008) 3003–3019.
[41] R. De Pascalis, M. Destrade, A. Goriely, Nonlinear correction to the Euler buckling formula for compressed cylinders with guided-guided end conditions, J. Elasticity 102 (2) (2011) 191–200.
[42] P. Wang, F. Casadei, S. Shan, J.C. Weaver, K. Bertoldi, Harnessing buckling to design tunable locally resonant acoustic metamaterials, Phys. Rev. Lett. 113 (1) (2014) 014301.
[43] K.F. Graff, Wave Motion in Elastic Solids, Courier Corporation, 2012.
[44] R. De Pascalis, M. Destrade, G. Saccomandi, The stress field in a pulled cork and some subtle points in the semi-inverse method of nonlinear elasticity, Proc. R. Soc. Lond. Ser. A Math. Phys. Eng. Sci. 463 (2087) (2007) 2945–2959.
[45] T. Shearer, W.J. Parnell, I.D. Abrahams, Antiplane wave scattering from a cylindrical cavity in pre-stressed nonlinear elastic media, Proc. R. Soc. Lond. Ser. A Math. Phys. Eng. Sci. 471 (2182) (2015) 20150450.
[46] W.J. Parnell, A.N. Norris, T. Shearer, Employing pre-stress to generate finite cloaks for antiplane elastic waves, Appl. Phys. Lett. 100 (17) (2012) 171907.
[47] W.J. Parnell, Nonlinear pre-stress for cloaking from antiplane elastic waves, Proc. R. Soc. Lond. Ser. A Math. Phys. Eng. Sci. 468 (2138) (2012) 563–580.
[48] M. Mooney, A theory of large elastic deformation, J. Appl. Phys. 11 (9) (1940) 582–592.
[49] A. Goriely, M. Destrade, M. Ben Amar, Instabilities in elastomers and in soft tissues, Quart. J. Mech. Appl. Math. 59 (4) (2006) 615–630.
[50] R. Mangan, M. Destrade, Gent models for the inflation of spherical balloons, Int. J. Non-Linear Mech. 68 (2015) 52–58, Mechanics of Rubber - in Memory of Alan Gent.
[51] L.R.G. Treloar, The Physics of Rubber Elasticity, Oxford University Press on Demand, 2005.
[52] K. Deb, A. Pratap, S. Agarwal, T. Meyarivan, A fast and elitist multiobjective genetic algorithm: NSGA-II, IEEE Trans. Evol. Comput. 6 (2) (2002) 182–197.
[53] ModeFRONTIER 2014, Update 1, version number 4.6.1 b20150227, 2014, User Manual.
[54] H. Guo, W.H. Hsu, GA-hardness revisited, in: E. Cantú-Paz, J.A. Foster, K. Deb, L.D. Davis, R. Roy, U.-M. O'Reilly, H.-G. Beyer, R. Standish, G. Kendall, S. Wilson, M. Harman, J. Wegener, D. Dasgupta, M.A. Potter, A.C. Schultz, K.A. Dowsland, N. Jonoska, J. Miller (Eds.), Genetic and Evolutionary Computation — GECCO 2003, Springer Berlin Heidelberg, Berlin, Heidelberg, 2003, pp. 1584–1585.
[55] M. Bodaghi, A.R. Damanpack, G.F. Hu, W.H. Liao, Large deformations of soft metamaterials fabricated by 3D printing, Mater. Des. 131 (2017) 81–91.
[56] T.D. Ngo, A. Kashani, G. Imbalzano, K.T.Q. Nguyen, D. Hui, Additive manufacturing (3D printing): A review of materials, methods, applications and challenges, Composites B 143 (2018) 172–196.
[57] C.J. Naify, A. Ikei, C.A. Rohde, Locally programmable metamaterial elements using four-dimensional printing, Extreme Mech. Lett. 36 (2020) 100654.
[58] Y. Jiang, Q. Wang, Highly-stretchable 3D-architected mechanical metamaterials, Sci. Rep. 6 (2016) 34147.
[59] G. Marckmann, E. Verron, Comparison of hyperelastic models for rubber-like materials, Rubber Chem. Technol. 79 (5) (2006) 835–858.
[60] L.Y.L. Ang, Y.K. Koh, H.P. Lee, Acoustic metamaterials: A potential for cabin noise control in automobiles and armored vehicles, Int. J. Appl. Mech. 08 (05) (2016) 1650072.
[61] C.-Y. Lee, M.J. Leamy, J.H. Nadler, Frequency band structure and absorption predictions for multi-periodic acoustic composites, J. Sound Vib. 329 (10) (2010) 1809–1822.
[62] M.R. Zarastvand, M. Ghassabi, R. Talebitooti, Acoustic insulation characteristics of shell structures: A review, Arch. Comput. Methods Eng. (2019) 1–19.
[63] R. De Pascalis, I.D. Abrahams, W.J. Parnell, Predicting the pressure–volume curve of an elastic microsphere composite, J. Mech. Phys. Solids 61 (4) (2013) 1106–1123.
[64] N. Gupta, S.E. Zeltmann, V.C. Shunmugasamy, D. Pinisetty, Applications of polymer matrix syntactic foams, JOM 66 (2) (2014) 245–254.